



FPI observations of nighttime mesospheric and thermospheric winds in China and their comparisons with HWM07

W. Yuan¹, X. Liu^{1,2}, J. Xu¹, Q. Zhou^{3,4}, G. Jiang¹, and R. Ma¹

¹State Key Laboratory of Space Weather, Center for Space Science and Applied Research, Chinese Academy of Sciences, Beijing 100190, China

²College of Mathematics and Information Science, Henan Normal University, Xinxiang 453007, China

³School of Electrical Engineering, Zhengzhou University, Zhengzhou 450001, China

⁴Electrical and Computer Engineering Department, Miami University, Oxford, OH, USA

Correspondence to: X. Liu (xliu@spaceweather.ac.cn)

Received: 24 February 2013 – Revised: 4 July 2013 – Accepted: 5 July 2013 – Published: 7 August 2013

Abstract. We analyzed the nighttime horizontal neutral winds in the middle atmosphere (~ 87 and ~ 98 km) and thermosphere (~ 250 km) derived from a Fabry–Perot interferometer (FPI), which was installed at Xinglong station (40.2° N, 117.4° E) in central China. The wind data covered the period from April 2010 to July 2012. We studied the annual, semiannual and terannual variations of the midnight winds at ~ 87 km, ~ 98 km and ~ 250 km for the first time and compared them with Horizontal Wind Model 2007 (HWM07). Our results show the following: (1) at ~ 87 km, both the observed and model zonal winds have similar phases in the annual and semiannual variations. However, the HWM07 amplitudes are much larger. (2) At ~ 98 km, the model shows strong eastward wind in the summer solstice, resulting in a large annual variation, while the observed strongest component is semiannual. The observation and model midnight meridional winds agree well. Both are equatorward throughout the year and have small amplitudes in the annual and semiannual variations. (3) There are large discrepancies between the observed and HWM07 winds at ~ 250 km. This discrepancy is largely due to the strong semiannual zonal wind in the model and the phase difference in the annual variation of the meridional wind. The FPI annual variation coincides with the results from Arecibo, which has similar geomagnetic latitude as Xinglong station. In General, the consistency of FPI winds with model winds is better at ~ 87 and ~ 98 km than that at ~ 250 km. We also studied the seasonally and monthly averaged nighttime winds. The most salient features include the following: (1) the seasonally averaged zonal winds at ~ 87 and ~ 98 km typically have

small variations throughout the night. (2) The model zonal and meridional nighttime wind variations are typically much larger than those of observations at ~ 87 km and ~ 98 km. (3) At ~ 250 km, model zonal wind compares well with the observation in the winter. For spring and autumn, the model wind is more eastward before $\sim 03:00$ LT but more westward after. The observed nighttime zonal and meridional winds on average are close to zero in the summer and autumn, which indicates a lack of strong stable tides. The consistency of FPI zonal wind with model wind at ~ 250 km is better than the meridional wind.

Keywords. Meteorology and atmospheric dynamics (climatology; middle atmosphere dynamics; thermospheric dynamics)

1 Introduction

Fabry–Perot interferometers (FPIs) play an important role in observing and studying the middle- (~ 87 and ~ 98 km) and upper-thermospheric (~ 250 km) winds. The global distribution of FPI has been listed in Table 1 of Drob et al. (2008). The thermospheric winds at ~ 250 km derived from 12 FPIs are important ground-based observational data to construct the new-generation Horizontal Wind Model 2007 (HWM07) (Drob et al., 2008). The middle-atmospheric wind data from Mount John (44.0° S, 170.4° E) and the South Pole are also included in HWM07. Beside the wind data from FPI, data from radar, rocket and other ground-based instruments, and satellites, as well as simulation data from a thermosphere–

ionosphere–mesosphere–electrodynamics general circulation model (TIME-GCM), are also incorporated into HWM07. As it stands now, HWM07 can provide horizontal neutral winds from ground to an altitude of 500 km. Moreover, the responses of neutral winds to geographical location, local time, season, geomagnetic activity, and the seasonal variability of tides and planetary waves can also be described by HWM07. The horizontal neutral wind models are, respectively, HWM07 and DWM07 during geomagnetic quiet conditions and storm times. It should be noted that both the effects of solar activities and interplanetary magnetic field, which have significant influences on the thermosphere wind (Emmert et al., 2006a, b), have not been included in HWM07 and DWM07.

Compared to the previous versions, HWM07 has incorporated much more ground-based observational data. However, there are few data coming from middle latitudes except for Mount John (geographic latitude: 44.0° S; geomagnetic latitude: 52.0° S) and Millstone Hill (geographic latitude: 42.6° N; geomagnetic latitude: 53.1° N), and Arecibo (geographic latitude: 18.4° N; geomagnetic latitude: 29.1° N). Although Mount John and Millstone Hill are at middle geographical latitudes, their geomagnetic latitudes are large. The thermospheric winds over Mount John and Millstone Hill are likely more affected by aurora heating from high latitude (Hagan, 1993) than those over Xinglong. On the other hand, since the Arecibo station is located at low geographical latitude and middle geomagnetic latitude, the thermospheric winds over Arecibo have typical characteristics of middle latitudes (Emmert et al., 2006a).

It should be noted that HWM07 has not incorporated the middle-atmospheric wind data over Arecibo. Moreover, HWM07 has not included the middle- and upper-thermospheric wind data from ground-based observations over China either. Consequently, it is necessary to examine the applicability of HWM07 over middle latitudes. Since the non-migrating atmospheric tides can cause the longitudinal variations of middle-atmospheric and upper-thermospheric winds (Lühr et al., 2007; Häusler and Lühr, 2009; Talaat and Lieberman, 2010; Forbes et al., 2012; Wu et al., 2012), it is important to observe the middle-atmospheric and upper-thermospheric wind by FPI over China. The observed winds are helpful to study the dynamics of middle and upper thermosphere, and to improve the accuracy of middle- and upper-thermosphere models.

There are many studies on middle-atmospheric wind based on radar and lidar observations and satellite observations (e.g., Dartt et al., 1983; Kazimirovsky and Vergasova, 2009; Shepherd et al., 2012). Whereas observational studies on thermospheric winds are confined to the data from a few incoherent scatter radar (ISR), FPI, and satellite observations (e.g., Drob et al., 2008; Emmert et al., 2006a, b, 2008; Santos et al., 2011; Wu et al., 2012; Shepherd et al., 2012). It has been generally accepted that the middle-atmospheric winds at middle latitudes are mainly influenced by the states

of the lower atmosphere and are less influenced by solar and geomagnetic activities (Kazimirovsky and Vergasova, 2009). However, global thermospheric winds are influenced by lower atmospheric waves, solar and geomagnetic activities, as well as the interplanetary magnetic field (e.g., Emmert et al., 2006a, b; Oberheide and Forbes, 2008). The thermospheric winds at ~ 250 km derived from FPIs at 7 stations are employed by Emmert et al. (2006a, b) to study the responses of thermospheric winds to local time, latitude, season and solar cycle during the geomagnetic quiet time ($K_p < 3$). They showed that wind speeds increase with the solar EUV radiation (measured by the 10.7 cm solar radiation flux) at high latitudes and in the geomagnetic equatorial region, and decrease with the solar EUV at middle latitudes (e.g., Millstone Hill and Arecibo). The responses of thermospheric winds are saturated when $F_{10.7} > 150$. However, Brum et al. (2012) showed that the saturation effect does not occur when a different solar activity proxy F_{107P} ($= (F_{10.7a} + F_{10.7})/2$) is used (here $F_{10.7a}$ is the 81-day average of $F_{10.7}$). Brum et al. (2012) ascribed this to the different proxies since the thermospheric wind variability is affected both by solar EUV and UV heating, which can be represented better by F_{107P} . Emmert et al. (2006a, b) also showed that the nighttime meridional wind was equatorward with a peak of $\sim 50 \text{ ms}^{-1}$ around 22:00 LT at low latitudes, whereas it can be as large as $150\text{--}200 \text{ ms}^{-1}$ during 00:00–03:00 LT at middle and high latitudes. As for the nighttime zonal wind, it was mainly eastward with a peak of $\sim 150 \text{ ms}^{-1}$. Emmert et al. (2006a) have shown that the thermospheric zonal wind over Arecibo exhibited annual variation during solar minimum and exhibited semiannual variation during solar maximum.

A FPI was installed at the Xinglong station (geographic location: 40.2° N, 117.4° E; geomagnetic location: 29.8° N, 193.2° E) of the National Astronomical Observatory in Hebei Province, China (Yuan et al., 2010). We have performed some preliminary studies based on the FPI data. Firstly, we compared the FPI winds during the period of 5 April–12 May 2010 with HWM93 (Yuan et al., 2010). Our comparisons showed that the winds from FPI agreed well with those from HWM93 at the altitudes of ~ 87 and ~ 98 km and exhibited apparent semidiurnal variations. However, there is a large discrepancy between the winds from FPI and HWM93 at ~ 250 km. Secondly, the winds at the altitude of ~ 87 km simultaneously measured from FPI and meteor radar at Beijing (~ 100 km away from FPI, e.g., Yu et al., 2013) during April–May 2010 are compared with HWM07 (Jiang et al., 2012). The monthly averaged nighttime winds from FPI, meteors, and HWM07 exhibit a similar trend except for some discrepancy in the meridional winds. Jiang et al. (2012) also showed that the meridional winds from FPI and meteor radar exhibit periodical oscillations with a period of 5 days. These comparisons indicate that our FPI is a reliable instrument to measure the middle-atmospheric winds.

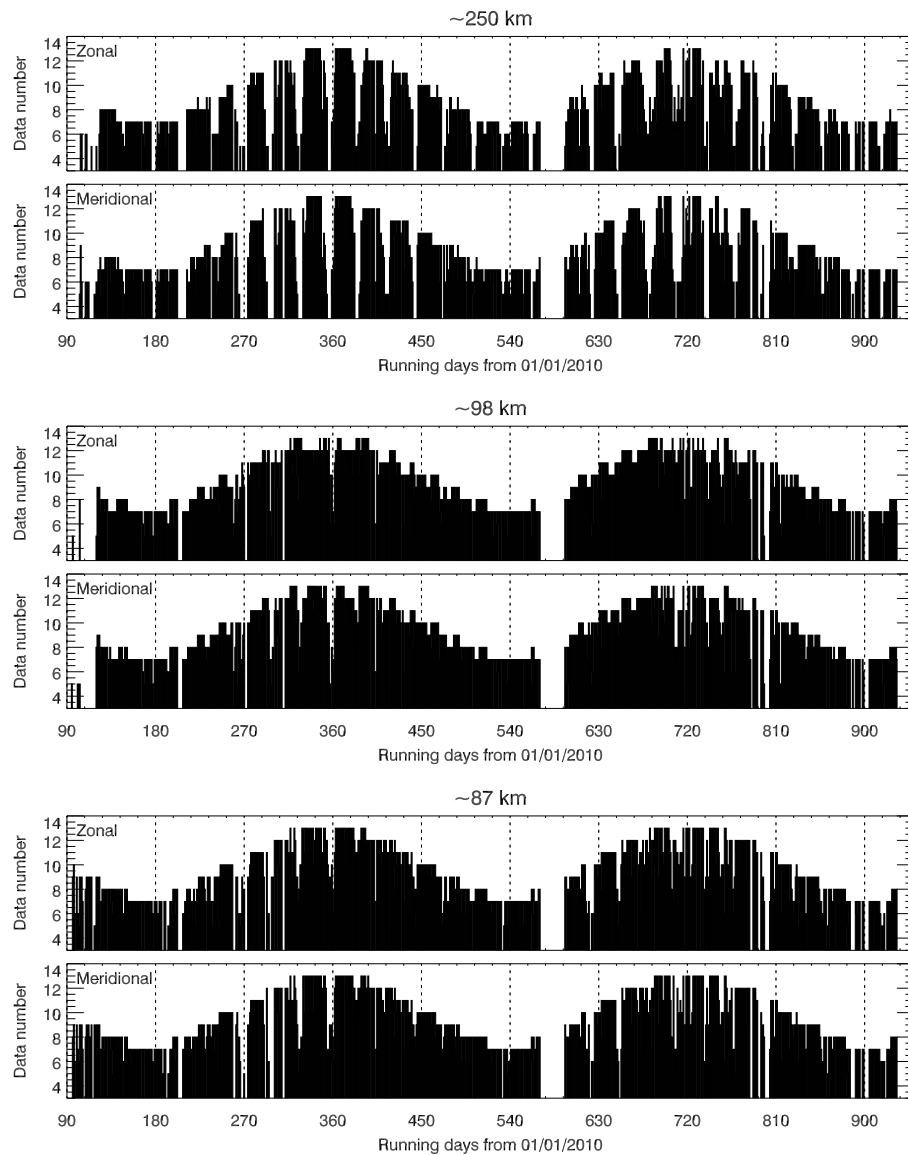


Fig. 1. Distributions of the valid data numbers in zonal and meridional winds in each night at the three airglow layers during April 2010–July 2012.

The wind data from our FPI used for this study cover a period of over two years since 2010. The length of the data allows us to study the long-term variations (e.g., annual, semi-annual, and terannual variations) of nighttime winds. One purpose of this paper is to study the long-term variations of the midnight winds in the middle atmosphere (~ 87 and ~ 98 km) and thermosphere (~ 250 km) over China. This is because there are more data at midnight. Assuming a constant tidal phase, selecting the midnight data can exclude the variations caused by tides. The other purpose is to analyze the seasonal variations of nighttime winds. Moreover, both the long-term variations of the midnight wind and the seasonal variations of nighttime winds will be compared with the winds from HWM07 to examine the applicability of

HWM07 over China. In our comparisons, the geomagnetic activity (three-hour A_p index) over this period is substituted in HWM07.

2 Instrument and data

The FPI installed at Xinglong station was in operation regularly since April 2010. It measured the airglow radiations from three layers: OH 892.0 nm, OI 557.7 nm and OI 630.0 nm. For each airglow layer, five directions (one zenith direction and four cardinal directions) at an elevation angle of 45° are measured in sequence (zenith, east, west, north, and south) in one duty cycle. The exposure time in each direction

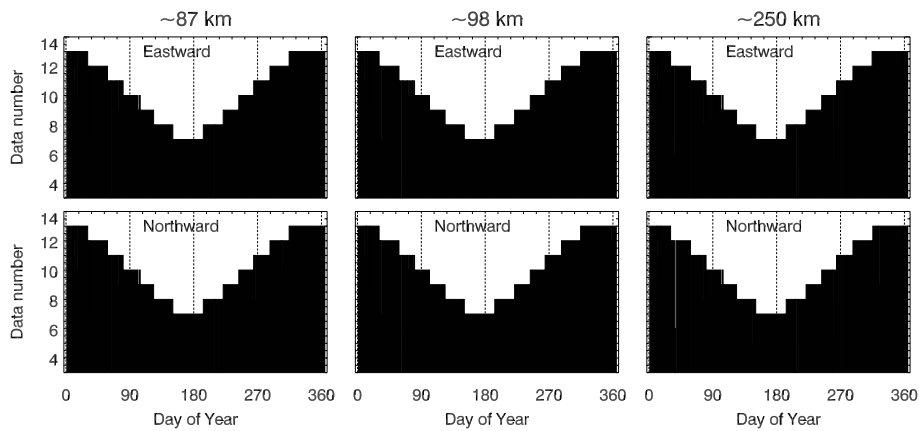


Fig. 2. Distributions of the valid data numbers in zonal and meridional winds in each night at the three airglow layers after binning all the data into one year with respect to the day number.

of one cycle is 3 min for OH 892.0 nm and OI 557.7 nm, and 5 min for OI 630.0 nm. Thus, the time resolution is ~ 1 h (Jiang et al., 2012). From the interference patterns of airglow radiations, horizontal winds at the altitudes of ~ 87 , ~ 98 and ~ 250 km are derived with a time interval of ~ 1 h. A detailed description of the FPI and data processing method can be found in Wu et al. (2004) and Yuan et al. (2010).

Here, we concentrate on the distributions of the available wind data from April 2010 to July 2012. Firstly, this study employed the winds at ~ 87 , ~ 98 , and ~ 250 km, which are derived from the airglow radiations of OH 892.0 nm, OI 557.7 nm, and OI 630.0 nm, respectively. Secondly, the criteria to select valid data are as follows (Yuan et al., 2010; Jiang et al., 2012): (1) the observed standard deviation (STD) is less than 40 m s^{-1} ; (2) the wind speed is less than 150 m s^{-1} ; and (3) there are at least 5 data points (approximately 5 h of observation) per night. The distributions of the valid data numbers of the zonal and meridional hourly winds in each night from April 2010 to July 2012 at the altitudes of ~ 87 , ~ 98 and ~ 250 km are presented in Fig. 1. The gap during May–August 2011 was due to instrument problems. As expected, there are more available data in the winter months due to the long nights. The numbers of valid hourly data points are ~ 12 – 13 (approximately 12–13 h of observation) around winter solstice.

To study the annual variations of midnight winds and the seasonal variations of nighttime winds, and to offset the missing data in some days, we binned all the valid data having the same date from different years to have a yearly composite. We note that the binned data reduce the statistical error to some extent but may increase the observational variability. The numbers of the valid data binned to one year are shown in Fig. 2. It can be seen that the binned data cover the entire year except for a few missing days.

The wind data from HWM07 are also used in this study. It should be noted that HWM07 included the effects of geomagnetic activities (input parameters are the three-hour

Ap index) but exclude the effects of solar activities (F10.7) and interplanetary magnetic field. To compare the winds from FPI and HWM07, we applied the three-hour Ap index (from ftp://ftp.ngdc.noaa.gov/STP/GEOMAGNETIC_DATA/INDICES/KP_AP/) into the HWM07 model. In Fig. 3, we plot the temporal evolutions F10.7 during April 2010–July 2012 (Fig. 3a) and the binned F10.7 over the three years (Fig. 3b). Figure 3 shows the large variability of F10.7 during our observation period. The daily averaged Ap index shows that this period is geomagnetically quiet in general except for three storms ($50 \leq \text{Ap} < 100$). The sample data during storms are too scarce to resolve the responses of thermospheric wind (~ 250 km) to geomagnetic activities. Thus, this will not be discussed here.

3 Annual variations of midnight winds and comparisons with HWM07

The vertical structures and variations of middle-atmospheric wind have been studied extensively using observations from ground-based instruments (e.g., rocket, radar and lidar) and satellite observations. However, comprehensive studies related to the temporal evolutions of the winds both in the middle atmosphere and in thermosphere are scarce. Although it has been reported that the seasonal variation of thermospheric wind is symmetric with respect to winter solstice, it has a large difference between the two equinoxes (Emmert et al., 2006a). Consequently, it is important to study the middle and thermospheric winds, their seasonal characteristics and their variations with local time. Moreover, comparison between the observations and model wind is helpful to understand and improve middle- and upper-atmospheric wind models.

The midnight winds ($00:00 \text{ LT} \pm 1 \text{ h}$) are chosen to compare with those from HWM07 since (1) there are more data at midnight; (2) the winds averaged over a local time interval

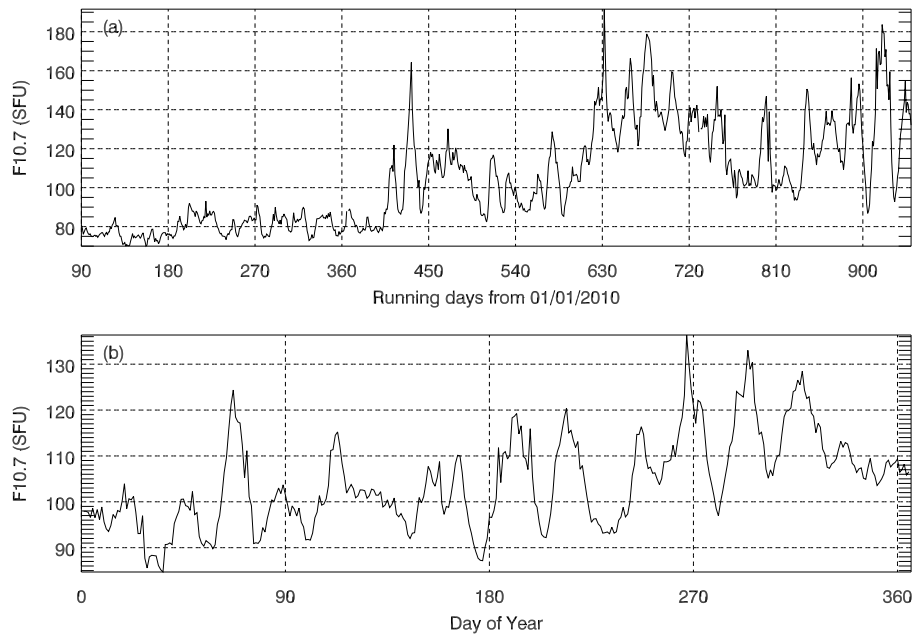


Fig. 3. Temporal evolutions of F10.7 during April 2010–July 2012 **(a)** and the binned F10.7 over the three years **(b)**.

can reduce the tidal effects. In Fig. 4, we present the midnight winds obtained from FPI (black dot) and HWM07 (green dot) at altitudes of ~ 87 , ~ 98 , and ~ 250 km. To make the data distribution more visible, we omitted the error bars of the midnight winds from FPI in Fig. 4. The typical error associated with the measurement can be found in Yuan et al. (2010) and Jiang et al. (2012). In Fig. 4, we also presented the monthly averaged winds as red triangles with the error bars indicating the monthly variability. The error bar is the STD of the same data used to calculate the monthly mean.

To study the long-term variations of midnight winds, we performed least-square (LS) harmonic fittings (Lomb, 1976) with annual, semiannual, and terannual components to the midnight winds shown in Fig. 4. The sums of all the harmonic components are shown as black lines for FPI winds in Fig. 4. Moreover, the variations with annual (solid line), semiannual (dash line), and terannual (dash dot line) components, as well as the annual mean wind (dot line) at three heights from FPI (black) and HWM07 (red) are shown in Fig. 5. The amplitudes and phases of each component from harmonic fit to the winds at three heights from FPI and HWM07 are listed in Table 1. The phase is the day of year when the zonal (eastward positive) or meridional (northward positive) wind achieves its maximum value.

3.1 Midnight winds at ~ 87 km

The zonal (eastward positive) and meridional (northward positive) winds at ~ 87 km shown in Fig. 4 indicate that observed winds generally have smaller variability, as indicated by the error bars, from the vernal equinox to the summer sol-

stice than in the winter months. This contrast is more noticeable in the meridional than in the zonal wind. The variation of the monthly averaged zonal wind from FPI coincides well with that from HWM07. Both of them exhibit similar annual and semiannual variations with respect to phases. However, the amplitudes of the periodical variations are larger in HWM07. As indicated in Table 1 and Fig. 5, the HWM07 annual- and semiannual-variation amplitudes are more than twice of those observed. The observed and model midnight zonal winds have eastward DC biases of 6 ms^{-1} and 10 ms^{-1} respectively. The smaller amplitude in the observation may be due to the fact that the airglow layer has a thickness of over 10 km and the vertical wavelength of tides is relatively short.

The monthly averaged meridional wind from FPI is weak throughout the year. Nevertheless, the meridional winds of the model and FPI from autumn equinox to vernal equinox largely agree with each other, while the agreement is not so good in the other half year. The long-term variations in the observation are mainly annual and terannual even though both have small amplitudes. In contrast, the meridional wind from HWM07 is dominated by an annual variation with an amplitude of 21 ms^{-1} , far exceeding the FPI amplitude of 11.4 ms^{-1} . The model midnight meridional wind also has a larger (15 ms^{-1}) southward DC bias than the observation (8 ms^{-1}) (since the data is not the daily average, the bias does not necessarily mean that the prevailing wind in the model is more southward). The large annual variation and the southward DC bias in the model wind results from a 40 ms^{-1} surge around summer solstice. Despite the large difference in

Table 1. Amplitudes and phases of annual, semiannual, and terannual variations for FPI and HWM07 winds (DoY = day of year).

Altitude (km)	Period (year)	Zonal wind				Meridional wind			
		Amplitude (m s^{-1})		Phase (DoY)		Amplitude (m s^{-1})		Phase (DoY)	
		FPI	HWM07	FPI	HWM07	FPI	HWM07	FPI	HWM07
~ 87	1	7.6	19.1	10	8	11.4	21.0	361	356
	1/2	11.0	24	182	181	0.8	2.7	32	81
	1/3	2.9	1.1	43	60	4.8	0.3	69	60
~ 98	1	3.7	14.3	107	175	4.1	3.4	302	264
	1/2	8.1	10.9	174	154	5.5	5.3	55	76
	1/3	1.6	0.2	50	19	1.2	0.2	61	117
~ 250	1	23.0	21.3	2	329	7.0	17.8	238	326
	1/2	5.9	23.2	18	67	3.3	15.6	151	76
	1/3	0.4	1.8	102	113	2.9	0.1	21	39

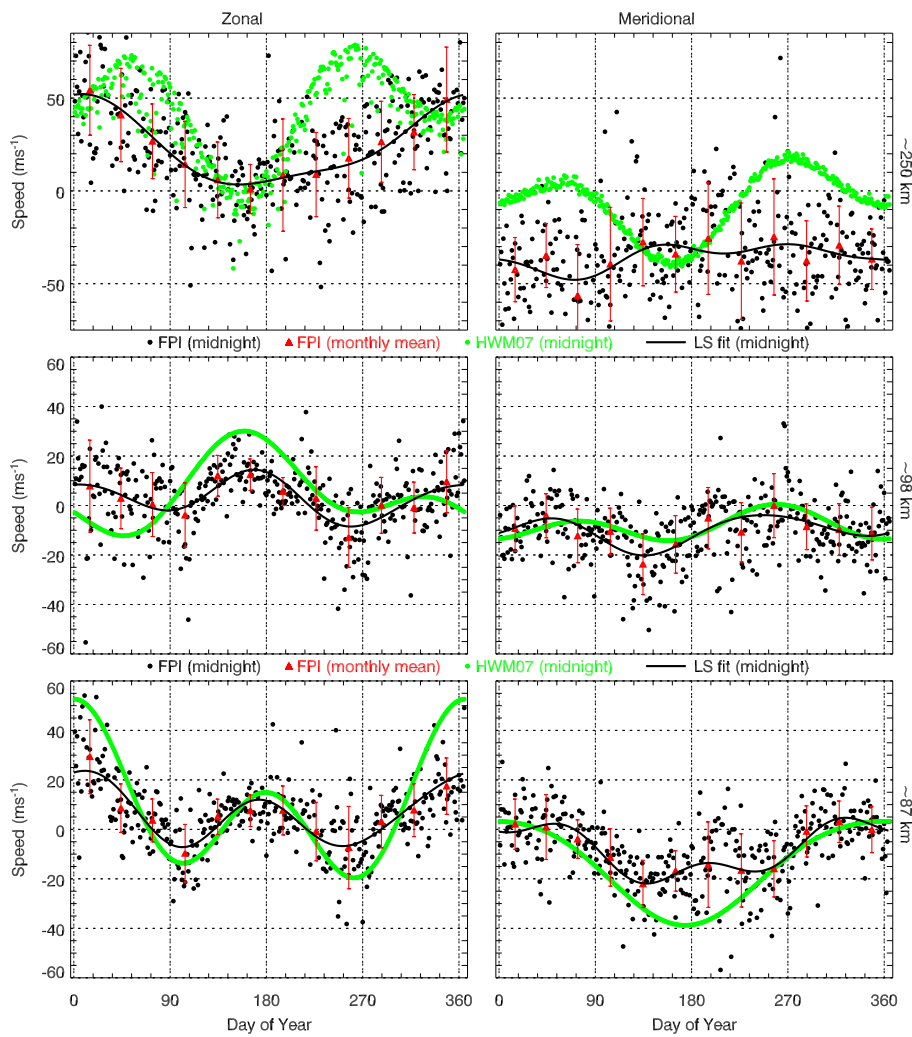


Fig. 4. Midnight zonal (eastward positive) and meridional (northward positive) winds obtained from FPI (black dot) and HWM07 (green line) at the altitudes of ~ 87 km (lower row), ~ 98 km (middle row), and ~ 250 km (upper row), respectively. The monthly averaged winds and their standard deviations are shown as red triangles and error bars.

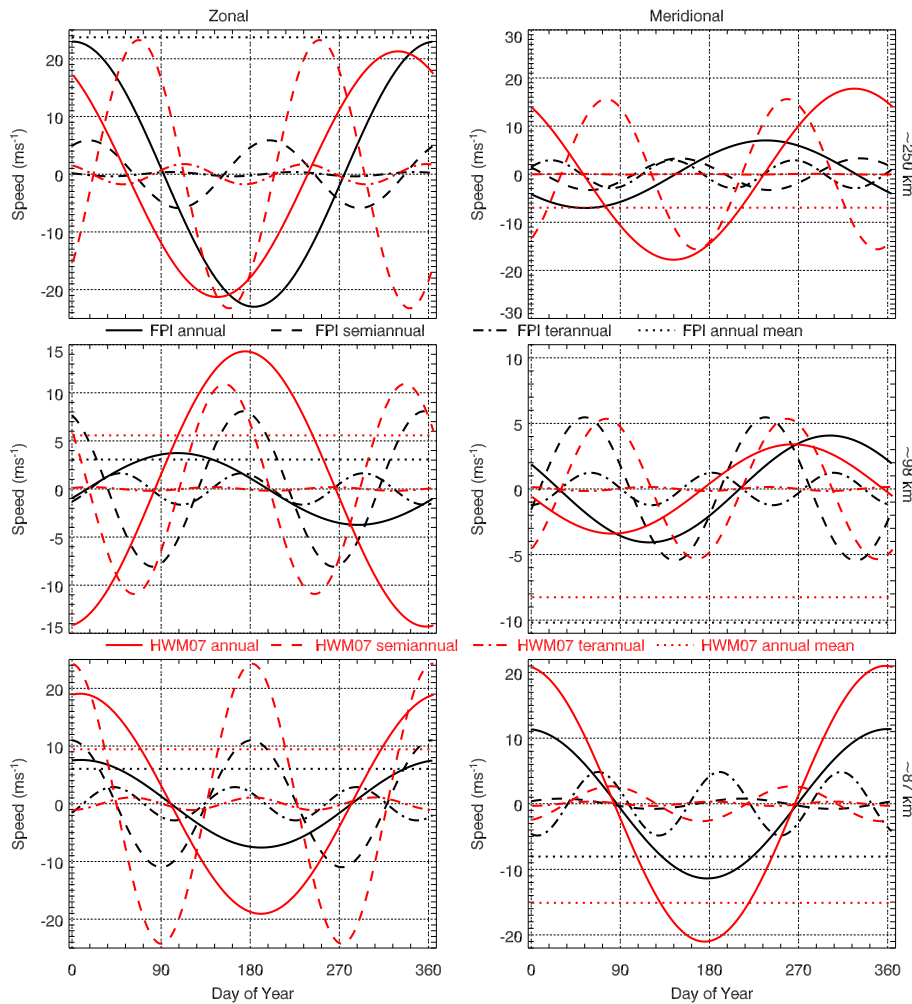


Fig. 5. Harmonic components of annual (solid line), semiannual (dash line), and terannual (dash dot line) variations and the annual mean (dot line) for midnight zonal (eastward positive) and meridional (northward positive) winds obtained from FPI (black) and HWM07 (red) at the altitudes of ~ 87 km (lower row), ~ 98 km (middle row), and ~ 250 km (upper row), respectively. The annual midnight model zonal wind mean and observation meridional wind are, respectively, 39.7 and -35.7 m s^{-1} , which are out of the plotted range in Fig. 5.

amplitude, the model and FPI phases in the annual variation are nevertheless in agreement.

Comparison of the winds from the FPI and a meteor radar 100 km away (Yu et al., 2013) with HWM07 shows that, although the meridional wind from FPI has a similar trend as that from meteor radar, the observed FPI and meteor radar winds are weaker than the wind from HWM07 (Fig. 4 of Jiang et al., 2012). Using a much longer data set here, our results also show that the observed wind is generally weaker than the model wind. One potential reason for the weaker FPI wind, as mentioned before, is that the airglow layer is relatively thick compared to the vertical wavelengths in this region.

3.2 Midnight winds at ~ 98 km

The zonal and meridional winds from FPI at ~ 98 km have similar STD as those at ~ 87 km throughout the year. The day-to-day variability in general appears to be consistent throughout the year except in the zonal wind in spring. The strongest component in the observed zonal wind is the semi-annual variation, while the strongest component in the model is the annual variation. The phases of the semiannual variation between the observation and the model agree reasonably well, while they are very different in the annual variation of zonal wind. Generally speaking, the model zonal wind agrees with the observation around the equinoxes, while the largest difference occurs around the solstices. In the meridional wind, the overall agreement is very good even though it appears that there is a slight phase difference between the model and the observation. The harmonic analysis suggests

that the moderate phase difference is mainly in the semi-annual variation of both zonal and meridional wind and in the annual variation of meridional wind. We note that unlike zonal wind (and the zonal and meridional winds at ~ 87 km), the observed amplitudes of both annual and semiannual variations in the meridional wind are slightly larger than those in the model.

As the centroids of the OH 892.0 nm (~ 87 km) and OI 557.7 nm (~ 98 km) airglow layers are only separated by 11 km, comparison between the results from the two layers may shed light on the vertical wavelength of the dominant oscillation. The observed zonal winds between the two heights are well correlated and their difference is not substantial. This indicates that the vertical wavelength in this region is likely longer than 20 km. The meridional winds from January to July between the two layers do not show substantial difference either. However, from August to December, the signs of meridional winds between the two heights are largely opposite, indicating potentially a much shorter wavelength during those months.

3.3 Midnight winds at ~ 250 km

Figure 4 shows that the distributions of the midnight zonal and meridional winds at ~ 250 km vary greatly from one day to another. The large variability in the thermospheric winds can be induced by the solar activity, geomagnetic activity and interplanetary field (Smith et al., 1994; Killeen et al., 1995; Richmond et al., 2003; Emmert et al., 2006a, b; Drob et al., 2008). In contrast, the variability of the model wind is not as significant as the FPI wind. One contributing factor for the discrepancy of the winds between our observation and the model is that HWM07 included the influence of geomagnetic activity (A_p index) but excluded the influences of solar activity and interplanetary magnetic field. It should be noted that the solar activity dependence of thermospheric wind has been explored by Emmert et al. (2006a, b) and Brum et al. (2012). Brum et al. (2012) also showed that the dependence of thermospheric wind on solar activity varies with local time and seasons. As seen from Fig. 3, the solar activity measured by F10.7 exhibits some variabilities during our observation period. The dependence is especially sensitive around midnight (see Fig. 6 of Brum et al., 2012). Ion drag can further cause additional variability in the thermospheric winds, especially in the seasonal variability.

Figure 4 indicates FPI and model zonal midnight winds are eastward throughout the year. They agree during the solstices but disagree during the equinoxes. The model shows strong enhancement during the equinoxes, which is lacking in our observation. The strong eastward wind during the equinoxes makes the semiannual variation a dominant feature in the model. The midnight meridional wind in the observation is strongly equatorward and shows only small fluctuations around a mean value of -36 m s^{-1} . Although the model wind also shows a southward bias, its mean value is much

smaller at -7 m s^{-1} . As in the zonal wind, the largest discrepancy between the model and the observation occur during the equinoxes. The variations of observed and model winds from January to July are further seen to be anti-correlated. The southward meridional wind in the midnight thermosphere over the Northern Hemisphere is controlled by the circulation from Equator to polar region at daytime and from polar region to Equator at nighttime (Witasse et al., 1998; Emmert et al., 2006a, b), which agrees with our observation.

The amplitudes of long-term variations listed in Table 1 show that the zonal and meridional winds from FPI exhibit strong annual variation and weak semiannual and terannual variations. In contrast, both the zonal and meridional winds from HWM07 exhibit strong annual and semiannual variations. As seen from Fig. 4, the strong semiannual variations in the model are due to the enhancement of eastward and southward winds during the equinox in the model. The phase of the model annual variation agrees largely with that of the observation in the zonal component but disagrees with observation in the meridional component. It should be noted that the data used in this study are from the period of increasing solar activity (see Fig. 3). Moreover, we should bear in mind the fact that the meridional wind shows large variability. The geomagnetic latitude of Xinglong station is similar to the Arecibo station despite their geographical latitudes differing substantially. The trend and phase of the annual variations of the ~ 250 km winds over Xinglong station are similar to those over Arecibo (as seen from Figs. 5 and 9 of Emmert et al., 2006a), while the wind amplitudes seem different between the two sites. Similarity with the thermospheric wind at ~ 250 km over Arecibo suggests possible influence of the geomagnetic field on thermospheric winds.

Comparison at the three heights shows that the degree of consistency of midnight winds between FPI and HWM07 is worse at ~ 250 km than at ~ 87 and ~ 98 km. This is mainly because the influences of solar activity and interplanetary magnetic field on middle-atmospheric winds are weaker than on thermospheric winds. Our comparison suggests that it is necessary to parameterize the effects of solar activity and interplanetary magnetic field when one develops thermospheric wind models.

4 Seasonal average nighttime wind and comparisons with HWM07

To complement the seasonal variation of the midnight winds, we discuss the nighttime variations of the wind in different seasons in this section. In this study, the corresponding months for spring, summer, autumn, and winter are 2-3-4, 5-6-7, 8-9-10, and 11-12-1, respectively. The two equinoxes and the two solstices are in the center of the corresponding seasons. The seasonally averaged nighttime zonal and meridional winds from FPI and HWM07 at the altitudes of ~ 87 , ~ 98 , ~ 250 km are shown in Figs. 6 and 8, respectively. The

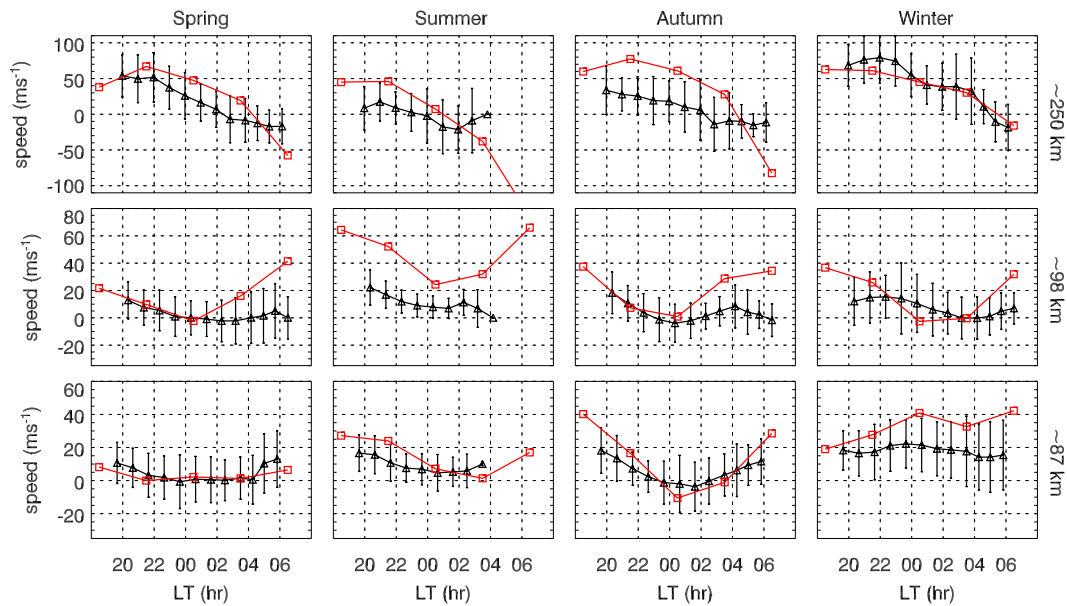


Fig. 6. Seasonally averaged nighttime zonal (eastward positive) wind from FPI (black triangle) and HWM07 (red square) in spring (first column), summer (second column), autumn (third column), and winter (fourth column) at the altitudes of ~ 250 km (first row), ~ 98 km (second row), and ~ 87 km (third row). The error bars are calculated from the standard deviation of the data points used for the seasonal average.

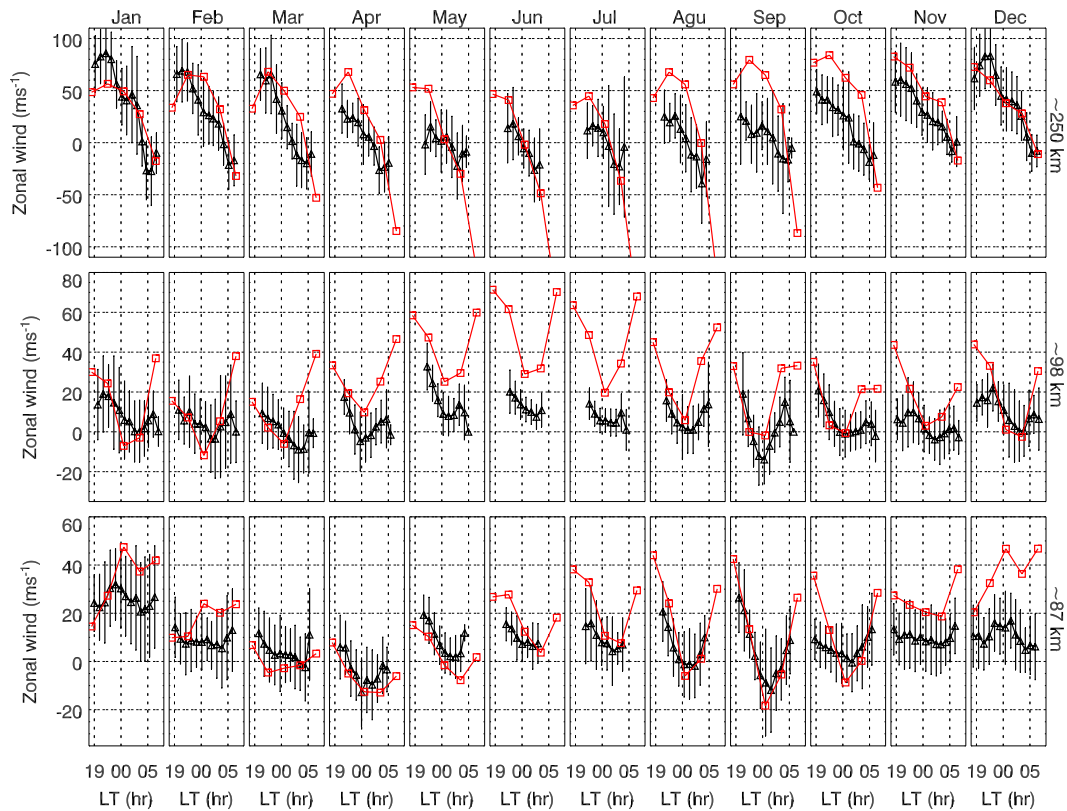


Fig. 7. Same as Fig. 6 but for the monthly average (eastward positive).

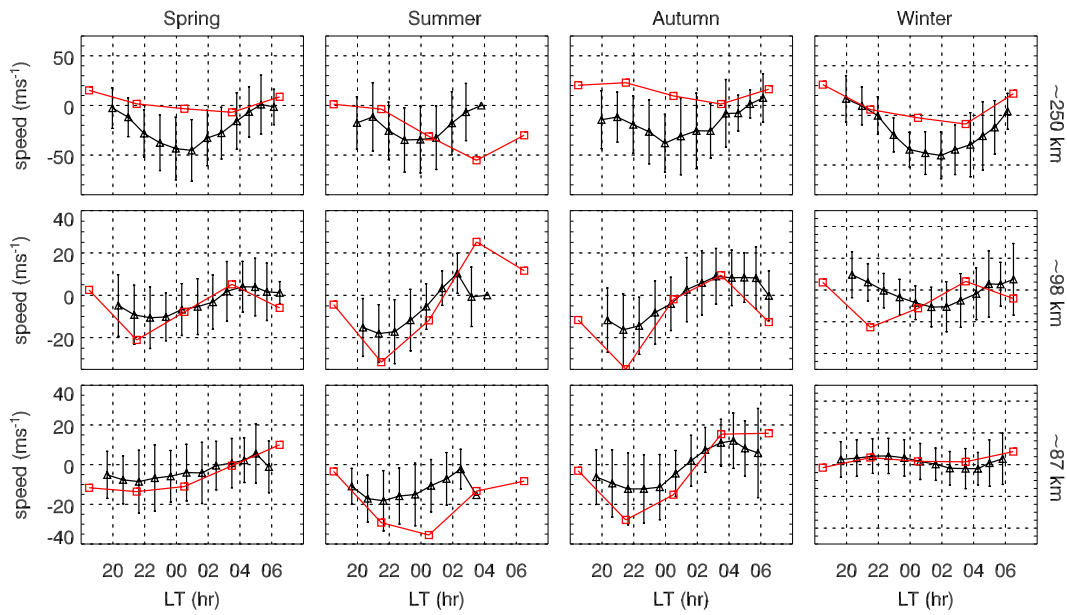


Fig. 8. Same as Fig. 6 but for the meridional (northward positive) wind.

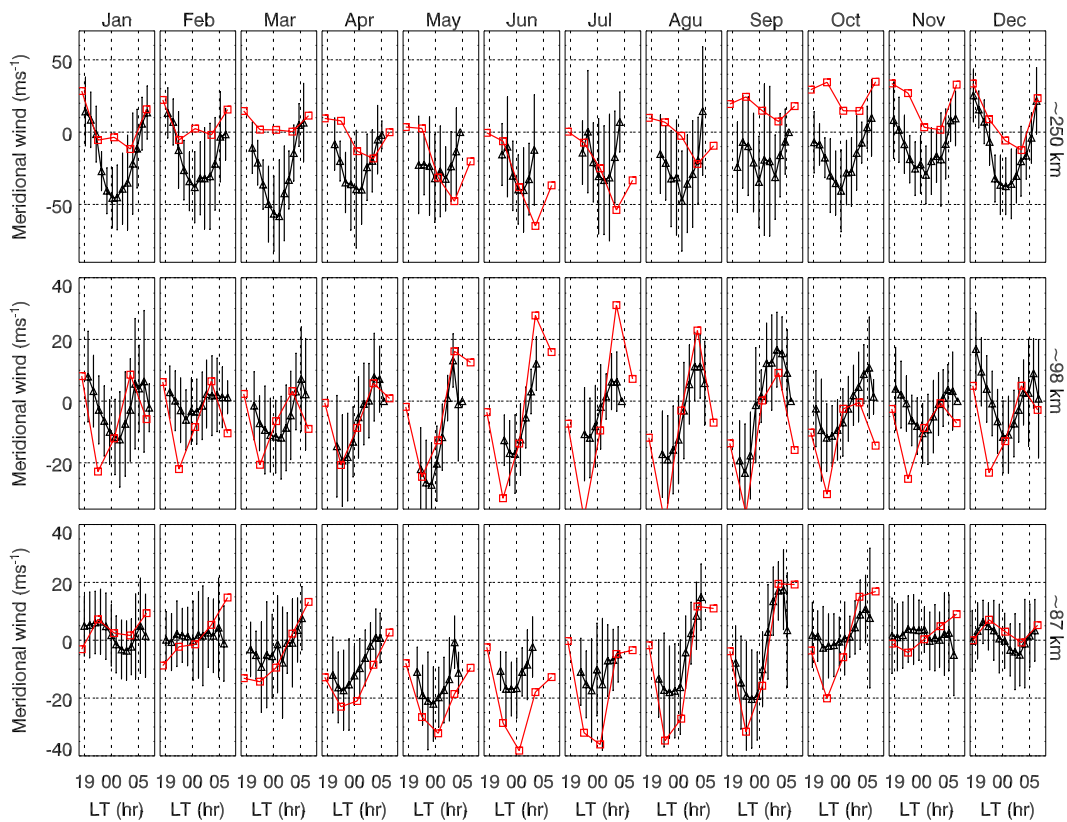


Fig. 9. Same as Fig. 7 but for the meridional (northward positive) wind.

error bars in each panel of Figs. 6 and 8 are calculated from the standard deviation of the data points used for the seasonal average. It illustrates the variability of the winds at the corre-

sponding local time. In the following, we discuss the nighttime variations of the seasonally averaged nighttime winds at the three altitudes in turn.

At ~ 87 km, the seasonally averaged nighttime variations are generally very weak in the zonal and meridional winds from FPI as seen from Figs. 6 and 8. In contrast, the HWM07 nighttime variations are apparent in summer and autumn. To understand the lack of nighttime variation in the seasonally averaged winds, we plot in Figs. 7 and 9 the monthly average of the zonal and meridional winds, respectively. As seen from Fig. 7, the nighttime variation of FPI zonal wind in most of the months (except August and September) does not fluctuate significantly, while the month-to-month variation is significant. Although our observation is limited to nighttime only, it appears that the zonal wind variation at 87 km is more controlled by annual and semiannual variations than by tides. The lower panel of Fig. 9 shows that the tidal amplitude in the meridional wind in the observation appears to be very small as well from October to March. The most significant nighttime variations, presumably caused by tides, occur from spring to autumn equinox. Unlike observations, the model winds exhibit strong nighttime variation, especially around autumn equinox.

Other than the fact that the airglow emission layer has a certain thickness, the nighttime variations at ~ 87 km are further likely weakened by the superposition of atmospheric waves with different periods, such as gravity wave, migrating and non-migrating tides, and planetary wave (Yuan et al., 2010; Jiang et al., 2012). These waves have different phases and/or their phases vary with time. Moreover, the periods of tides may not be exactly 24 h, 12 h, etc. As a result, the superposition of these waves may offset the nighttime variations on the timescale of a season. The lack of strong tides in our observation warrants further investigation.

At ~ 98 km, the observed winds exhibit stronger nighttime variations than at ~ 87 km although their amplitudes are less than those in HWM07 at 98 km (especially in the middle panels of Figs. 7 and 9). Unlike the winds at 87 km, the observed nighttime variation is larger than the annual variation. The model eastward wind shows a sharp turn around midnight, decreasing before and increasing after midnight very quickly. This “V”-shaped characteristic is largely reflected in the monthly averaged observation although the observed amplitude of variation is much smaller and the timing of minimum eastward is often after midnight. Also the observation does not show the zonal wind being strongly biased eastward as the model does in the summer months. The monthly averaged meridional wind compares very favorably with the model wind as seen in Fig. 9. The nighttime variation of meridional winds in the model and observation very much depends on the season (as seen in the middle panel of Figs. 8 and 9). From Fig. 9, we can find that, in the winter months from November to February, the observed meridional wind is northward in the early evening and early dawn hours while it is southward around midnight. In the summer months, the meridional wind changes from strong southward to strong northward during the few hours around midnight. The night-

time variations in the winds from FPI at ~ 98 km indicate that there are relatively stable tides at this height.

For the zonal wind at ~ 250 km, Fig. 6 shows that the observed and model zonal winds agree best in the winter. The observed and model zonal winds for all seasons switch from eastward to westward during the night. The direction-switching time in the model is typically around 04:00 LT with the exception in the summer when the switching time occurs shortly after midnight. The direction-switching time in the observation around the solstices agrees with the model. In fact, Fig. 7 shows that around the solstices in June–July and December–January, FPI and model zonal winds largely agree throughout the night except around 22:00 LT in December–January when the observation shows an eastward peak wind of $\sim 85 \text{ m s}^{-1}$. Around equinoxes, the direction-switching time in the FPI is about 2 h ahead the model (as shown in Figs. 6 and 7). The observation also shows a much smaller amplitude variation in the summer months (from April to September in Fig. 7) than in the winter months. This indicates that the tides are either weaker or have a less stable phase from spring to autumn equinox than the other months.

For the meridional wind at ~ 250 km, the nighttime variation of the observed wind is apparent and has a strong southward peak during 00:00–02:00 LT from October to April, as seen from Fig. 9. In comparison, the model nighttime variation has a similar trend but much weaker amplitude. From May to September, the nighttime variation of the observed wind is weak, but the model wind shows large variations. It should be noted that the seasonally averaged nighttime variations of our zonal and meridional winds generally agree with the results from Arecibo, which is located at a similar geomagnetic latitude as Xinglong station (see Fig. 5 of Emmert et al., 2006a, and Fig. 8 of Brum et al., 2012), except for the differences in wind amplitudes of the two sites. Moreover, the southward wind in the thermospheric nighttime wind is similar to that obtained from ten years of observations of MU radar at Shigaraki, Japan (34° N , 136° E) (Kawamura et al., 2000).

The nighttime variations of the seasonally averaged winds at ~ 250 km indicate that there are strong tides at this height in winter and spring. Moreover, the tides have a relatively stable phase. Otherwise, the superposition of nighttime wind at different days may be offset in one season and will not exhibit nighttime variations. We should note that the strong diurnal tide in the meridional wind has been explored by the MU radar at Shigaraki, Japan (34° N , 136° E) (Kawamura et al., 2000). Because we have only nighttime data available, we have not attempted to delineate the dominant tidal modes. Tidal analysis is further complicated by the existence of terdiurnal component, which can compete with diurnal and semidiurnal tides as shown by Gong and Zhou (2011) using incoherent scatter radar data. Thermospheric tides can be generated in situ or in the lower and middle atmosphere, as discussed by Müller-Wodarg et al. (2001). Our data unfortunately do not allow us to delineate which tidal generation

mechanism is stronger. Nevertheless, the data presented here do provide a qualitative assessment of the overall seasonal tidal amplitude at the three airglow heights.

5 Summary and conclusions

The wind data at the altitudes of ~ 87 , ~ 98 , and ~ 250 km measured from FPI over Xinglong, China, from April 2010 to July 2012 are analyzed. The winds are also compared with HWM07 including the effects of geomagnetic activity (three-hour A_p index). We studied the annual, semiannual, and terannual variations of the midnight winds in the middle atmosphere (~ 87 and ~ 98 km) and thermosphere (~ 250 km). Moreover, we also studied the variations of seasonally and monthly averaged nighttime winds at the three airglow altitudes.

The long-term characteristics of the observed midnight winds and their comparisons with the HWM07 are summarized below:

1. At 87 km, the zonal wind shows annual and semiannual variations with an amplitude of about 10 m s^{-1} for both components, while the meridional wind exhibits annual and terannual variation with an amplitude of 11.4 and 4.8 m s^{-1} , respectively. The two strongest long-term variations in the HWM07 zonal wind are semiannual and annual as in the observation, and they have the same phases as the observation. The long-term variation of the HWM07 meridional wind is largely annual and its phase agrees well with the observation. The model typically has much larger amplitude than the observation, which may be due to the fact that the airglow layer has a thickness not much narrower than the vertical wavelengths of tides at this altitude. The largest discrepancy at this altitude between the model and the observation is the presence of strong southward wind in the model in the summer months.
2. At 98 km, the strongest observed long-term variation in both zonal and meridional winds is semiannual. The strongest model long-term variation is annual in the zonal wind, while it is semiannual in the meridional wind. The phases of the model and observed semiannual variations agree, while the phases of the annual variations do not agree. The largest discrepancy between model and observation is in the zonal wind annual variation.
3. At 250 km, the FPI zonal and meridional winds are dominated by the annual variation. Unlike the observation, the amplitudes of the semiannual and annual variations in zonal or meridional wind are similar. The semiannual variations in the model are due to enhancement in the eastward (northward) wind during the equinoxes. Other than the annual variation in the zonal wind, the

observed midnight wind variations largely do not agree with the model. It should be noted that the trend and phases of the annual variations in our observation are similar to those observed at Arecibo, which has a similar geomagnetic latitude to but a different geographical latitude than Xinglong, while the wind amplitudes are different between the two sites. This indicates the possible influence of geomagnetic field on thermospheric winds.

4. Comparing among the three layers, the consistency of FPI winds with model winds is better at ~ 87 and ~ 98 km than that at ~ 250 km.

Our study of the seasonally and monthly averaged nighttime variations reveals the following:

1. At 87 km, the nighttime variations of the FPI zonal and meridional winds are small from October to March. The largest variation in both zonal and meridional winds occurs in August and September. This suggests that tidal winds from October to March are either very small or their phases vary significantly within a month. The HWM07 zonal wind, however, shows relatively large nighttime variation most of the year, especially around autumn equinox. The FPI meridional wind compares well with the model most of the year except around summer solstice.
2. At 98 km, both the FPI and model eastward winds decelerate but remain largely positive before midnight for all the seasons. The model eastward wind accelerates after midnight, while FPI zonal wind is close to zero. The observed nighttime meridional wind shifts from southward to northward in spring, summer and autumn. For these three seasons, the model meridional wind compares well with the observation. In the winter, the observed meridional wind is southward around 02 LT but is northward after dusk and before dawn.
3. At 250 km, both the FPI and model zonal winds change almost monotonically from eastward to westward over night for all the seasons although the eastward-to-westward cross-over time in the observation is ahead of that of the model for all the seasons except winter. The FPI nighttime meridional wind throughout the year is predominantly southward, with the largest amplitude occurring around midnight. The FPI nighttime variations in both zonal and meridional winds are larger in winter and spring than in summer and autumn. The strong seasonal dependence of the nighttime observation suggests that thermospheric tides over Xinglong are likely much stronger and stable in winter–spring than in summer–autumn.
4. The seasonally averaged FPI zonal and meridional winds agree well with the model winds at 87 and \sim

98 km. The consistency of FPI zonal wind with the model wind at ~ 250 km is better than the meridional wind.

Acknowledgements. This work was supported by the Chinese Academy of Sciences (KZZD-EW-01-2) and the National Science Foundation of China (41229001, 41004063 and 41174127), and the National Important Basic Research Project (Grant No. 2011CB811405). This work was also supported in part by the Specialized Research Fund and Educational Commission of Henan Province of China (13A110547) and the Open Research Program of the State Key Laboratory of Space Weather, and by National Science Foundation of the United States grant ATM-0633418 and AGS1243133 to Miami University. We acknowledge the use of data from the Chinese Meridian Project.

Topical Editor C. Jacobi thanks two anonymous referees for their help in evaluating this paper.

References

- Brum, C. G. M., Tepley, C. A., Fentzke, J. T., Robles, E., dos Santos, P. T., and Gonzalez, S. A.: Long-term changes in the thermospheric neutral winds over Arecibo: Climatology based on over three decades of Fabry–Perot observations, *J. Geophys. Res.*, 117, A00H14, doi:10.1029/2011JA016458, 2012.
- Dartt, D., Nastrom, G., and Belmont, A.: Seasonal and solar cycle wind variations, 80–100 km, *J. Atmos. Terr. Phys.*, 45, 707–718, 1983.
- Drob, D. P., Emmert, J. T., Crowley, G., Picone, J. M., Shepherd, G. G., Skinner, W., Hays, P., Niecejewski, R. J., Larsen, M., She, C. Y., Meriwether, J. W., Hernandez, G., Jarvis, M. J., Sipler, D. P., Tepley, C. A., O'Brien, M. S., Bowman, J. R., Wu, Q., Murayama, Y., Kawamura, S., Reid, I. M., and Vincent, R. A.: An empirical model of the Earth's horizontal wind fields: HWM07, *J. Geophys. Res.*, 113, A12304, doi:10.1029/2008JA013668, 2008.
- Emmert, J. T., Faivre, M. L., Hernandez, G., Jarvis, M. J., Meriwether, J. W., Niecejewski, R. J., Sipler, D. P., and Tepley, C. A.: Climatologies of nighttime upper thermospheric winds measured by ground-based Fabry–Perot interferometers during geomagnetically quiet conditions: 1. Local time, latitudinal, seasonal, and solar cycle dependence, *J. Geophys. Res.*, 111, A12302, doi:10.1029/2006JA011948, 2006a.
- Emmert, J. T., Hernandez, G., Jarvis, M. J., Niecejewski, R. J., Sipler, D. P., and Vennerstrom, S.: Climatologies of nighttime upper thermospheric winds measured by ground-based Fabry–Perot interferometers during geomagnetically quiet conditions: 2. High-latitude circulation and interplanetary magnetic field dependence, *J. Geophys. Res.*, 111, A12303, doi:10.1029/2006JA011949, 2006b.
- Emmert, J. T., Drob, D. P., Hernandez, G., Jarvis, M. J., Meriwether, J. W., Niecejewski, R. J., Shepherd, G. G., Sipler, D. P., and Tepley, C. A.: DWM07 global empirical model of upper thermospheric storm-induced disturbance winds, *J. Geophys. Res.*, 113, A11319, doi:10.1029/2008JA013541, 2008.
- Forbes, J. M., Zhang, X., and Bruinsma, S.: Middle and upper thermosphere density structures due to nonmigrating tides, *J. Geophys. Res.*, 117, A11306, doi:10.1029/2012JA018087, 2012.
- Gong, Y. and Zhou, Q.: Incoherent scatter radar study of the terdiurnal tide in the E- and F- region heights at Arecibo, *Geophys. Res. Lett.*, 38, L15101, doi:10.1029/2011GL048318, 2011.
- Hagan, M. E.: Quiet time upper thermospheric winds over Millstone Hill between 1984 and 1990, *J. Geophys. Res.*, 98, 3731–3739, doi:10.1029/92JA01605, 1993.
- Häusler, K. and Lühr, H.: Nonmigrating tidal signals in the upper thermospheric zonal wind at equatorial latitudes as observed by CHAMP, *Ann. Geophys.*, 27, 2643–2652, doi:10.5194/angeo-27-2643-2009, 2009.
- Jiang, G. Y., Xu, J. Y., Yuan, W., Ning, B. Q., Wan, W. X., and Hu, L. H.: A comparison of mesospheric winds measured by FPI and meteor radar located at 40N, *Sci. China Tech. Sci.*, 55, 1245–1250, doi:10.1007/s11431-012-4773-1, 2012.
- Kawamura, S., Otsuka, Y., Zhang, S.-R., Fukao, S., and Oliver, W. L.: A climatology of middle and upper atmosphere radar observations of thermospheric winds, *J. Geophys. Res.*, 105, 12777–12788, 2000.
- Kazimirovsky, E. S. and Vergasova, G. V.: Mesospheric, lower thermospheric dynamics and external forcing effects: a review, *Indian J. Radio Space Phys.*, 38, 7–36, 2009.
- Killeen, T. L., Won, Y.-I., Niecejewski, R. J., and Burns, A. G.: Upper thermosphere winds and temperatures in the geomagnetic polar cap: Solar cycle, geomagnetic activity, and interplanetary magnetic field dependencies, *J. Geophys. Res.*, 100, 21327–21342, 1995.
- Lomb, N. R.: Least-square frequency analysis of unequally spaced data, *Astrophysics and Space Science*, 39, 447–462, 1976.
- Lühr, H., Häusler, K., and Stolle, C.: Longitudinal variation of F region electron density and thermospheric zonal wind caused by atmospheric tides, *Geophys. Res. Lett.*, 34, L16102, doi:10.1029/2007GL030639, 2007.
- Müller-Wodarg, I. C. F., Aylward, A. D., and Fuller-Rowell, T. J.: Tidal oscillations in the thermosphere: a theoretical investigation of their sources, *J. Atmos. Solar-Terr. Phys.*, 63, 899–914, doi:10.1016/S1364-6826(00)00202-9, 2001.
- Oberheide, J. and Forbes, J. M.: Tidal propagation of deep tropical cloud signatures into the thermosphere from TIMED observations, *Geophys. Res. Lett.*, 35, L04816, doi:10.1029/2007GL032397, 2008.
- Richmond, A. D., Lathuillere, C., and Vennerstrom, S.: Winds in the high-latitude lower thermosphere: Dependence on the interplanetary magnetic field, *J. Geophys. Res.*, 108, 1066, doi:10.1029/2002JA009493, 2003.
- Santos, P. T., Brum, C. G. M., Tepley, C. A., Aponte, N., González, S. A., and Robles, E.: Using incoherent scatter radar to investigate the neutral wind long-term trend over Arecibo, *J. Geophys. Res.*, 116, A00H13, doi:10.1029/2011JA016514, 2011.
- Shepherd, G. G., Thuillier, G., Cho, Y.-M., Duboin, M.-L., Evans, W. F. J., Gault, W. A., Hersom, C., Kendall, D. J. W., Lathuillere, C., Lowe, R. P., McDade, I. C., Rochon, Y. J., Shepherd, M. G., Solheim, B. H., Wang, D.-Y., and Ward, W. E.: The Wind Imaging Interferometer (WINDII) on the Upper Atmosphere Research Satellite: A 20 year perspective, *Rev. Geophys.*, 50, RG2007, doi:10.1029/2012RG000390, 2012.
- Smith, R. W., Hernandez, G., Price, K., Fraser, G., Clark, K. C., Schulz, W. J., Smith, S., and Clark, M.: The June 1991 Thermospheric Storm Observed in the Southern Hemisphere, *J. Geophys. Res.*, 99, 17609–17615, doi:10.1029/94JA01101, 1994.

- Talaat, E. R. and Lieberman, R. S.: Direct observations of nonmigrating diurnal tides in the equatorial thermosphere, *Geophys. Res. Lett.*, 37, L04803, doi:10.1029/2009GL041845, 2010.
- Witasse, O., Lilensten, J., Lathuillere, C., and Pibaret, B.: Meridional thermospheric neutral wind at high latitude over a full solar cycle, *Ann. Geophys.*, 16, 1400–1409, doi:10.1007/s00585-998-1400-3, 1998.
- Wu, Q., Gablehouse, R. D., Solomon, S. C., Killen, T. L., and She, C. Y.: A new Fabry-Perot interferometer for upper atmospheric research, *Proc. SPIE*, 5660, 218–227, 2004.
- Wu, Q., Ortland, D. A., Fostera, B., and Roble, R. G.: Simulation of nonmigrating tide influences on the thermosphere and ionosphere with a TIMED data driven TIEGCM, *J. Atmos. Sol-Terr. Phys.*, 90–91, 61–67, 2012.
- Yu, Y., Wan, W., Ning, B., Liu, L., Wang, Z., Hu, L., and Ren, Z.: Tidal Wind Mapping from observations of a meteor radar chain in December, 2011, *J. Geophys. Res.*, 118, doi:10.1029/2012JA017976, 2013.
- Yuan, W., Xu, J. Y., Ma, R. P., Wu, Q., Jiang, G. Y., Gao, H., Liu, X., and Chen, S. Z.: First observation of mesospheric and thermospheric winds by a Fabry-Perot interferometer in China, *Chinese Sci. Bull.*, 55, 4046–4051, doi:10.1007/s11434-010-4192-2, 2010.